Effects of Crank Length on the Dynamics Behavior of a Flexible Connecting Rod

Jen-San Chen
Professor

Chu-Hsian Chian
Graduate Student,

Department of Mechanical Engineering,
National Taiwan University,
Taipei, Taiwan 10617

Global dynamics behavior of a damped flexible connecting rod is considered in this paper with emphasis on the effects of the rigid crank length. Nonlinear equations of motion in terms of axial and transverse deflections are derived based on Lagrangian strain formulation. When the crank length is small compared to the connecting rod, it is found that only one periodic solution exists in the speed range up to 1.5 times the first bending natural frequency of the connecting rod. As the crank length increases, however, multiple solutions may exist and the associated domains of attraction can be identified by cell-to-cell mapping technique. Moreover, the steady state response may become chaotic, which renders precise prediction of the dynamics response meaningless. The onset rotation speed of chaotic vibration decreases when the crank length increases. This result shows that previous research utilizing simplified or linearized models can predict the dynamics response of the flexible connecting rod only when both the crank length and the rotation speed are small. [DOI: 10.1115/1.1368882]

Introduction

The flexible connecting rod of a slider-crank mechanism can be considered as a beam undergoing large rigid body motion and may deform in both the axial and transverse directions. Previous research of interest includes transient vibration, steady state response, and dynamic stability analysis. A complete formulation should take into account the coupling effect of the axial and transverse vibrations. However, due to mathematical complexity, it was very common in the past to adopt various assumptions in the formulation to facilitate analytical study. The simplest approach is to assume that the axial load in the connecting rod is a function of time only and can be obtained by assuming that the connecting rod is rigid. The resulted equation of motion in terms of the transverse deflection is an inhomogeneous Mathieu equation [1–7].

The second approach is to relate the axial force to the transverse displacement by integrating the axial equilibrium equation. This formulation is an improvement of the previous one, and has been adopted by Viscomi and Ayre [8], and Hsieh and Shaw [9]. The resulting equation in terms of the transverse deflection is nonlinear. Thompson and Sung [10] developed a nonlinear finite element theory and conducted experiments to verify their analytical predictions.

The third approach is to consider the effect of axial vibration, but assume that the axial force is proportional to the linear axial strain [11–13]. The two equations of motion involve both the axial and transverse deflections. To simplify the solution procedure the coupled equations of motion are then linearized by deleting all the terms containing products of deflections.

Recently Chen and Chen [14] reformulated the equations of motion of the flexible connecting rod by assuming that the axial force is proportional to the Lagrangian axial strain, which involves both the axial and transverse deflections. They found that previous simplified or linearized formulations considerably overestimate the transient response, especially when the crank speed is comparable to the first bending natural frequency of the connecting rod because terms of significant order of magnitude are ignored inadequately. In most of the publications cited above, the length of the rigid crank is assumed to be small to facilitate analytical study. To our best knowledge, the effects of crank length on the dynamic response of the connecting rod have not been discussed in detail yet.

In this paper we extend Chen and Chen's work [14] to consider the global dynamics behavior of a damped flexible connecting rod with emphasis on the effects of the rigid crank length. Complete nonlinear equations of motion in terms of axial and transverse deflections are derived based on Lagrangian strain formulation. Bifurcation diagrams based on Poincare mapping are presented. Multiple steady state solutions and the associated domains of attraction are studied by cell-to-cell mapping technique [15]. Possible chaotic responses of a flexible connecting rod with moderate and long crank lengths are demonstrated. It is believed that this interesting phenomenon has not been reported in the literature. The results from linear strain formulation are also presented for comparison.

Equations of Motion

Figure 1 shows a slider-crank mechanism. The rigid crank of length a rotates with constant speed Ω. The connecting rod is assumed to be made of a viscoelastic material. The length, cross section area, mass density, Young's modulus, and internal material damping of the connecting rod are L, A, ρ, E, and μ, respectively. The mass of the slider is m_s. XOY is an inertial frame with its origin attached to the center of the rotating crank. xAy is a moving frame with x-axis passing through the two ends of the connecting rod. $u(x,t)$ and $v(x,t)$ denote the axial and transverse deflections of the connecting rod. From the force balance in the axial and transverse directions and the moment balance of a small element of the connecting rod, we obtain three equilibrium equations,

$$P_{,x}=\rho A[u_{,tt}-2v_{,t}\dot{\phi}-(x+u)\dot{\phi}^2-v\ddot{\phi}-a\Omega^2\cos(\Omega t-\phi)] \tag{1}$$

$$Q_{,x}=\rho A[v_{,tt}+2u_{,t}\phi-v\dot{\phi}^2+(x+u)\ddot{\phi}-a\Omega^2\sin(\Omega t-\phi)] \tag{2}$$

$$M_{,x}+Q-Pv_{,x}=0 \tag{3}$$

P, Q, and M are the axial force, shear force, and bending moment, respectively, at position x on the connecting rod. ϕ is the angle between the x- and X-axes, and can be obtained from rigid body kinematics,

Contributed by the Technical Committee on Vibration and Sound for publication in the JOURNAL OF VIBRATION AND ACOUSTICS. Manuscript received February 2000; revised December 2000. Associate Editor: R. A. Ibrahim.

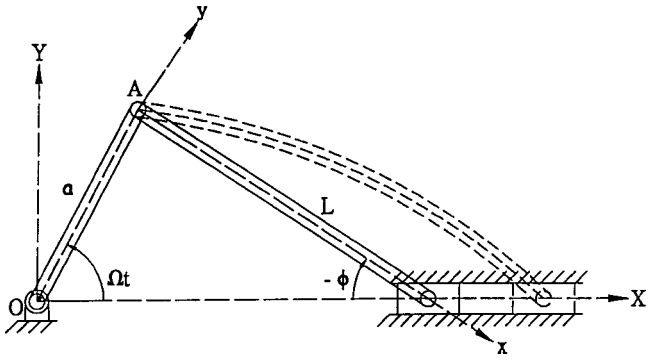

Fig. 1 Schematic diagram of a slider and crank mechanism

$$\phi=\sin^{-1}\left(-\frac{a\sin\Omega t}{L}\right) \tag{4}$$

The constitutive laws of an Euler beam are used,

$$P=EA\left(u_{,x}+\frac{1}{2}v_{,x}^2\right)+\mu A\left(u_{,x}+\frac{1}{2}v_{,x}^2\right)_{,t} \tag{5}$$

$$M=EIv_{,xx}+\mu Iv_{,xxt} \tag{6}$$

In Eq. (5) the axial force is assumed to be proportional to Lagrangian strain. I is the area moment of inertia of the connecting rod,

$$I=Ar^2$$

where r is the radius of gyration. By substituting Eqs. (3), (5), and (6) into Eqs. (1) and (2) we obtain the following equations of motion,

$$u_{,tt}-\dot\phi^2u-\frac{E}{\rho}(u_{,xx}+v_{,x}v_{,xx})-2\dot\phi v_{,t}-\ddot\phi v-x\dot\phi^2-a\Omega^2\cos(\Omega t-\phi)-\frac{\mu}{\rho}(u_{,xxt}+v_{,xt}v_{,xx}+v_{,x}v_{,xxt})=0 \tag{7}$$

$$v_{,tt}-\dot\phi^2v+\frac{EI}{\rho A}v_{,xxxx}+2\dot\phi u_{,t}+\ddot\phi u-\frac{E}{\rho}\left(u_{,xx}v_{,x}+u_{,x}v_{,xx}+\frac{3}{2}v_{,x}^2v_{,xx}\right)+\frac{\mu I}{\rho A}v_{,xxxxt}-\frac{\mu}{\rho}(u_{,xxt}v_{,x}+2v_{,xx}v_{,xt}v_{,x}+u_{,xt}v_{,xx}+v_{,x}^2v_{,xxt})+x\ddot\phi-a\Omega^2\sin(\Omega t-\phi)=0 \tag{8}$$

The connecting rod is assumed to be simply-supported at both ends. Therefore the boundary conditions for u and v are

$$v(0,t)=v(L,t)=v_{,xx}(0,t)=v_{,xx}(L,t)=u(0,t)=0 \tag{9}$$

From the force balance of the slider we can obtain the boundary condition for u at $x=L$.

$$\mu A\left(u_{,x}+\frac{1}{2}v_{,x}^2\right)_{,t}\Big|_{x=L}+EA\left(u_{,x}+\frac{1}{2}v_{,x}^2\right)\Big|_{x=L}=-\frac{1}{\cos\phi}\left[\frac{1}{2}\rho AL a\Omega^2\sin\phi\sin(\Omega t-\phi)-\frac{1}{3}\rho AL^2\ddot\phi\sin\phi+m_s(-a\Omega^2\cos\Omega t-L\dot\phi^2\cos\phi+a\ddot\phi\sin\Omega t)\right] \tag{10}$$

Nondimensionalization

Equations (7) and (8) can be nondimensionalized by introducing the following dimensionless quantities,

$$x^*=\frac{x}{L},\ a^*=\frac{a}{L},\ u^*=\frac{L}{r^2}u,\ v^*=\frac{v}{r},\ \varepsilon=\frac{r}{L},$$

$$m_s^*=\frac{m_s}{\rho AL},\ P^*=\frac{P}{EA},\ \Omega^*=\frac{\Omega}{\omega_b},\ t^*=\omega_bt,\ \mu^*=\frac{\mu r^2\pi^4}{\rho\omega_bL^4}$$

ω_b is the lowest bending natural frequency of the connecting rod,

$$\omega_b=\frac{\pi^2}{L^2}\sqrt{\frac{EI}{\rho A}}$$

The ratio between the bending natural frequency and the longitudinal natural frequency of the connecting rod is proportional to ε, the slenderness ratio parameter. After substituting these relations into Eqs. (7), (8), and (10), and dropping the superposed asterisks for simplicity, we can rewrite the equations of motion and the inhomogeneous boundary condition in the following forms,

$$\varepsilon^2(u_{,tt}-\dot\phi^2u)-\varepsilon(2\dot\phi v_{,t}+\ddot\phi v)-\frac{1}{\pi^4}(u_{,xx}+v_{,x}v_{,xx})-\frac{\mu}{\pi^4}(u_{,xxt}+v_{,xt}v_{,xx}+v_{,x}v_{,xxt})-x\dot\phi^2-a\Omega^2\cos(\Omega t-\phi)=0 \tag{11}$$

$$\varepsilon^2(2\dot\phi u_{,t}+\ddot\phi u)+\varepsilon\left[v_{,tt}-\dot\phi^2v+\frac{1}{\pi^4}\left(v_{,xxxx}-u_{,xx}v_{,x}-u_{,x}v_{,xx}-\frac{3}{2}v_{,x}^2v_{,xx}\right)\right]+\varepsilon\frac{\mu}{\pi^4}v_{,xxxxt}-\varepsilon\frac{\mu}{\pi^4}(u_{,xxt}v_{,x}+2v_{,xx}v_{,xt}v_{,x}+u_{,xt}v_{,xx}+v_{,x}^2v_{,xxt})+x\ddot\phi-a\Omega^2\sin(\Omega t-\phi)=0 \tag{12}$$

$$\frac{P(1,t)}{\varepsilon^2}=\mu\left(u_{,x}+\frac{1}{2}v_{,x}^2\right)_{,t}\Big|_{x=1}+\left(u_{,x}+\frac{1}{2}v_{,x}^2\right)\Big|_{x=1}=-\frac{\pi^4}{\cos\phi}(\Theta-m_sa\Omega^2\cos\Omega t) \tag{13}$$

where

$$\Theta=\frac{a}{3}\ddot\phi\sin\Omega t-\frac{1}{2}a^2\Omega^2\sin\Omega t\sin(\Omega t-\phi)+m_s(-\dot\phi^2\cos\phi+a\ddot\phi\sin\Omega t)$$

It is noted that by this scaling method the small parameter ε arises naturally, which can then be used to compare the order of magnitude of each term in the dimensionless equations.

We assume a one-mode approximation for u and v as following,

$$u(x,t)=f(t)\sin\frac{\pi x}{2} \tag{14}$$

$$v(x,t)=g(t)\sin\pi x \tag{15}$$

After substituting Eqs. (14) and (15) into Eqs. (11) and (12), multiplying Eqs. (11) and (12) by $\sin(\pi x/2)$ and $\sin\pi x$, respectively, and then integrating by parts from $x=0$ to 1 we obtain

$$\varepsilon^2(\ddot f-\dot\phi^2f)-\varepsilon\frac{8}{3\pi}(2\dot\phi\dot g+\ddot\phi g)+\frac{1}{\pi^2}\left(\frac{f}{4}+\frac{7}{15}g^2\right)+\frac{\mu}{\pi^2}\left(\frac{\dot f}{4}+\frac{14}{15}g\dot g\right)=\frac{8}{\pi^2}\dot\phi^2+\frac{4}{\pi}a\Omega^2\cos(\Omega t-\phi)-\frac{2}{\cos\phi}(\Theta-m_sa\Omega^2\cos\Omega t) \tag{16}$$

$$\varepsilon^2\frac{8}{3\pi}(2\dot\phi\dot f+\ddot\phi f)+\varepsilon\left(\ddot g-\dot\phi^2g+g+\frac{14}{15\pi^2}fg+\frac{3}{8}g^3\right)+\varepsilon\mu\left(\dot g+\frac{14}{15\pi^2}\dot fg+\frac{3}{4}g^2\dot g\right)=-\frac{2}{\pi}\ddot\phi+\frac{4}{\pi}a\Omega^2\sin(\Omega t-\phi) \tag{17}$$

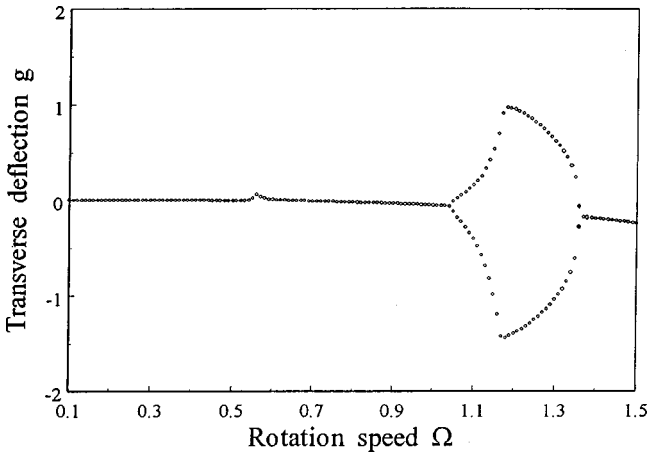

Fig. 2 Bifurcation diagram for crank length $a=0.1$. In the speed range $1.05<\Omega<1.37$ the solution is P-2.

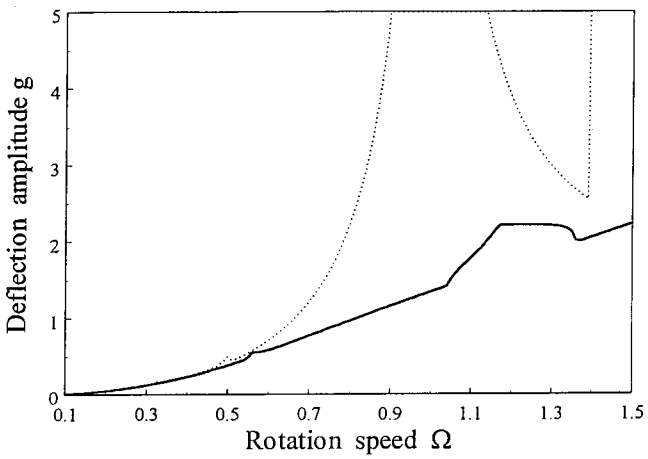

Fig. 3 Amplitude of the steady state transverse deflection g for crank length $a=0.1$. Solid and dotted lines represent the results from nonlinear and linear strain formulations, respectively.

In the case when the expression of linear strain is used in Eq. (5), Eqs. (16) and (17) should be changed to

$$\varepsilon^2(\ddot{f}-\dot{\phi}^2 f)-\varepsilon\frac{8}{3\pi}(2\dot{\phi}\dot{g}+\ddot{\phi}g)+\frac{f}{4\pi^2}+\frac{\mu}{4\pi^2}\dot{f}$$
$$=\frac{8}{\pi^2}\dot{\phi}^2+\frac{4}{\pi}a\Omega^2\cos(\Omega t-\phi)-\frac{2}{\cos\phi}$$
$$\times(\Theta-m_s a\Omega^2\cos\Omega t) \tag{18}$$

$$\varepsilon^2\frac{8}{3\pi}(2\dot{\phi}\dot{f}+\ddot{\phi}f)+\varepsilon\left(\ddot{g}-\dot{\phi}^2 g+g+\frac{14}{15\pi^2}fg\right)+\varepsilon\mu\left(\dot{g}\right.$$
$$\left.+\frac{14}{15\pi^2}\dot{f}g\right)=-\frac{2}{\pi}\ddot{\phi}+\frac{4}{\pi}a\Omega^2\sin(\Omega t-\phi) \tag{19}$$

Short Crank Length, $a=0.1$

Equations (16) and (17) are two nonlinear coupled equations with periodic coefficients and forcing terms. In the following sections we use Runge-Kutta method to study the steady state solutions of the flexible connecting rod. The time interval of the integration is chosen to be one-hundredth of the crank rotation period. Satisfactory convergence is always checked and ensured. We first choose the following parameters for a slider-crank mechanism with relatively short crank: $\varepsilon=0.05$, $\mu=0.024$, $m_s=0.1$, $a=0.1$. After specifying initial conditions for $f,\dot{f},g,\dot{g}$ at certain crank speed Ω, we examine the Poincare map of the response in the $g-\dot{g}$ space. The deflection is recorded when the crank is in the direction of the slider motion. If there exists a periodic steady state solution with frequency $n\Omega$, the points in the Poincare map converge to n separated points. We call this periodic steady state vibration a P-n solution [15]. With damping ratio $\mu=0.024$ the steady state solution can be reached after 300 cycles. We record these steady state solutions in Fig. 2 for another 100 cycles. In other words, each point for a periodic solution in Fig. 2 actually represents 100 points at the same location in the Poincare map. In the case when $a=0.1$, Fig. 2 shows that the P-1 solutions bifurcate to P-2 at $\Omega=1.05$, and then change back to P-1 again at $\Omega=1.37$. The Ω increment in the bifurcation diagram is 0.01. To examine whether different initial conditions result in different steady state solutions we choose four points in $f-\dot{f}$ space, $(f,\dot{f})=(\pm3,\pm3)$. For each of these points in $f-\dot{f}$ space, we choose 25 evenly-separated points in $g-\dot{g}$ space within the ranges $|g|\leq4.5$ and $|\dot{g}|\leq4.5$. For these 100 different initial conditions the solutions settle to the same steady states in this case. In other words, no multiple solution can be found in the specified range of initial conditions.

The amplitude of these periodic steady state vibrations can be recorded as the solid line in Fig. 3. The amplitude tends to be larger at higher rotation speed. In order to compare with the results from linear strain formulation, we plot the amplitude of the steady state vibration calculated from Eqs. (18) and (19) as the dotted line in Fig. 3. It is observed that linear strain formulation gives satisfactory results up to $\Omega=0.6$ for $a=0.1$. In the neighborhood of $\Omega=1$ the amplitude from linear strain formulation can reach more than 10 times of that predicted by nonlinear strain formulation. Furthermore, bounded steady state vibrations cannot be found with linear strain formulation when $\Omega>1.4$.

The physics behind the large discrepancies between the linear and nonlinear strain models in high-speed range may be explained in the following. First of all in the low speed range the deflection predicted by the linear strain model is quite small and the nonlinear effect of the Lagrangian strain model is negligible. When the rotation speed approaches the first bending natural frequency, on the other hand, the transverse deflection grows and the neutral axis of the connecting rod stretches. Consequently the axial tensile stresses developed within the connecting rod stiffen and add considerable resistance to bending deflection. This stiffening effect can only be modeled mathematically by the quadratic term in the Lagrangian strain.

Moderate Crank Length, $a=0.4$

We next consider a slider-crank mechanism with moderate crank length $a=0.4$ while the other parameters remain the same. Figure 4 shows the bifurcation diagram from Poincare sampling similar to Fig. 2. The same 100 initial conditions as in Fig. 2 are used in the calculation. It is noted that multiple periodic steady state vibrations exist. For instance, in the speed range $0.42<\Omega<0.46$ there exist two P-1 solutions. In Fig. 5 we choose the initial point $(f,\dot{f})=(0.5,0.5)$ and use cell-to-cell mapping techniques [15] to identify the domains of attraction of these two steady state solutions in the $g-\dot{g}$ space when $\Omega=0.43$. The $g-\dot{g}$ space is divided into 150×150 cells. The attractors for the two P-1 solutions are denoted by black dots. Steady state vibrations of these two attractors are shown in Fig. 6. The black dots on the curves denote the sampling time in Poincare mapping. It is noted that the basin boundary of the two attractors changes as the rotation speed of the rigid crank changes. Therefore, by fixing an initial point and changing rotation speed, the response may settle

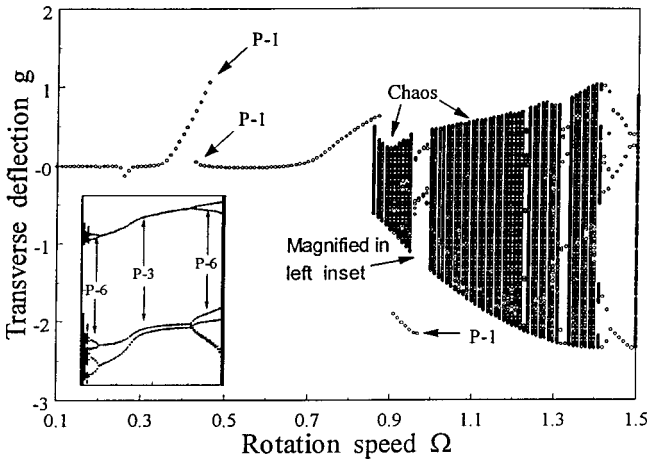

Fig. 4 Bifurcation diagram for crank length $a=0.4$. The response becomes chaotic when $\Omega>0.86$. The left inset is the magnification of speed range $0.96<\Omega<0.99$.

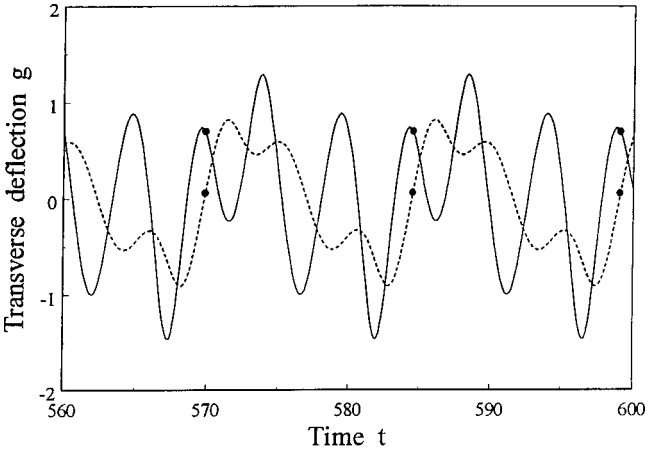

Fig. 6 Steady state vibrations of the two attractors in Fig. 5.

to a different attractor for a different speed. Although it is impractical trying to locate all the attractors in the entire state space, the 100 initial conditions should cover most of the responses for those initial points in the state space of interest. More initial points can always be examined whenever faster computing facility becomes available.

In the higher speed range $\Omega>0.86$, it is noted that the response becomes chaotic. After identifying chaotic response we record the deflections for 500 cycles in Fig. 4. In other words, each black strip in Fig. 4 represents 500 points on the Poincare map. In the speed range $0.86<\Omega<0.96$ one P-1 attractor and a chaotic attractor coexist. The onset of chaotic response at $\Omega=0.86$ is so abrupt that typical period doubling phenomenon was not observed even by an Ω increment of 0.0005. After ignoring the solutions of the first 300 cycles, the Poincare map at $\Omega=0.9$ with 60000 points is shown in Fig. 7. The typical fractal distribution can be observed.

In the speed range $0.96<\Omega<0.99$ the response becomes periodic again. We magnify this speed range with Ω increment of 0.0005 in the left inset of Fig. 4. These solutions belong to a single attractor undergoing period bifurcation from chaos to P-12, P-6, P-3, and back to P-6, P-12, and chaos again.

To examine how well the linear strain formulation works compared to the nonlinear one when $a=0.4$, we plot the steady state amplitudes from nonlinear and linear formulations as solid and dotted lines, respectively, in Fig. 8. It is noted that the linear strain formulation gives satisfactory results only when $\Omega<0.3$. In particular, the response from linear strain formulation becomes unbounded when the rotation speed is in the neighborhood of 0.48 and beyond 0.73.

Long Crank, $a=0.6$

We now consider the case of long rigid crank with $a=0.6$. The bifurcation diagram similar to Figs. 2 and 4 is shown in Fig. 9. Multiple solutions can be observed starting from $\Omega=0.49$, and chaotic response occurs as early as $\Omega=0.53$. The left inset in Fig. 9 is the magnification of speed range $0.51<\Omega<0.64$ with Ω increment equal to 0.0005. In this speed range one can observe an attractor (I) undergoing transition from chaotic to P-4, P-2, and finally to P-1. In the same speed range another attractor (II) bifurcates from P-1, to P-2, P-4, P-8, and finally becomes chaotic. The rotation speeds at which period bifurcation occurs can be recorded for these two attractors in Table 1 with Ω accuracy of 10^{-5}. Notation Ω_{m-n} represents the rotation speed at which P-m solution bifurcates to P-n solution. One can calculate the ratio

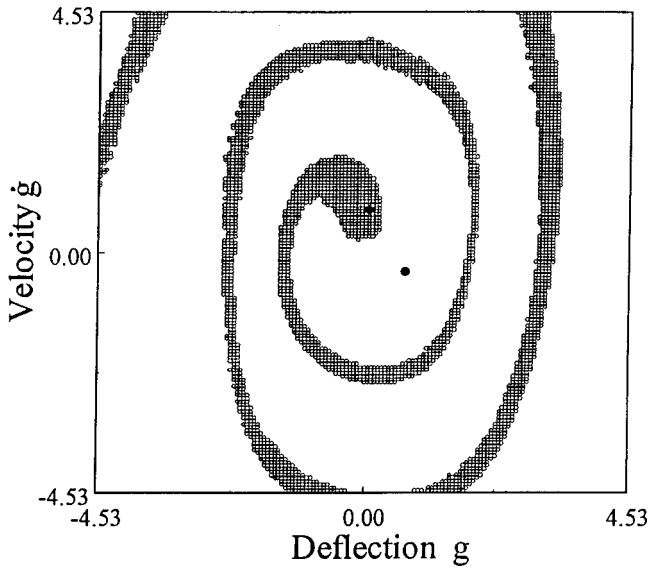

Fig. 5 Two domains of attraction when $\Omega=0.43$. The stable attractors are marked with black dots.

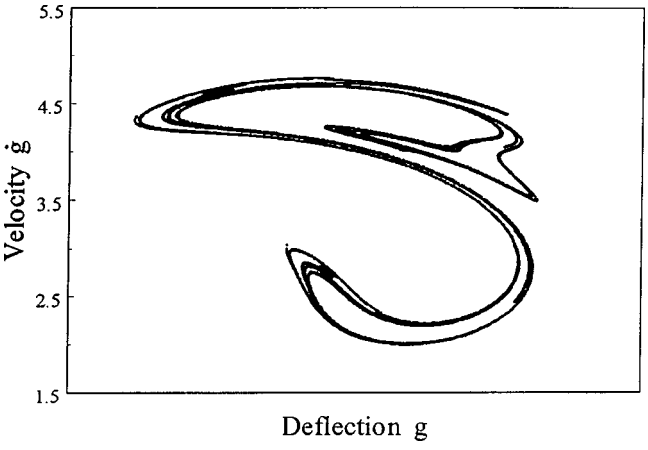

Fig. 7 Poincare map at $\Omega=0.9$ after the solutions of the first 300 cycles are ignored. 60000 points are recorded in this map.

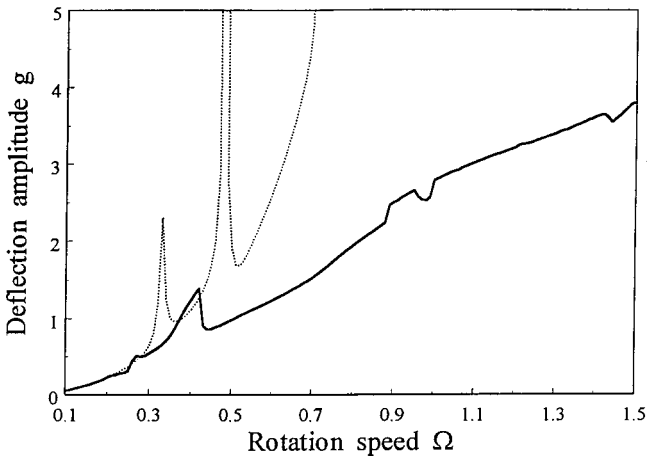

Fig. 8 Amplitude of the steady state transverse deflection g when crank length $a=0.4$. Solid and dotted lines represent the results from nonlinear and linear strain formulations, respectively.

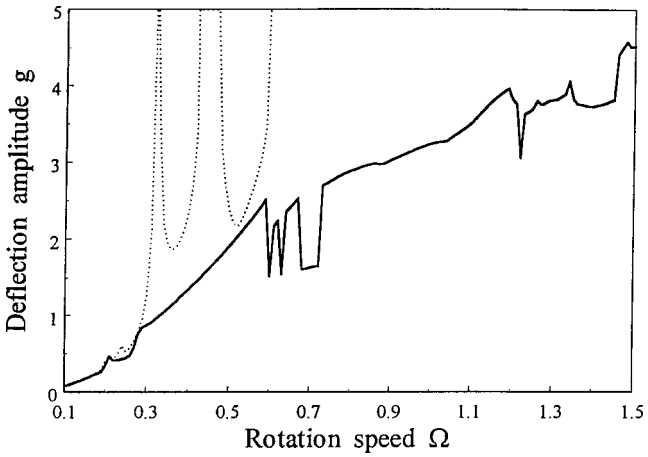

Fig. 10 Amplitude of the steady state transverse deflection g when crank length $a=0.6$. Solid and dotted lines represent the results from nonlinear and linear strain formulations, respectively.

$$\frac{\Omega_{8-16}-\Omega_{4-8}}{\Omega_{16-32}-\Omega_{8-16}}$$

for attractors I and II as 4.22727 and 4.57895, respectively. These two ratios are close to the well-known Feigenbaum number 4.66920 [16]. This indicates that the inherent mathematical structure of the current system is similar to a one-dimensional quadratic map.

Figure 10 shows the vibration amplitude from both nonlinear and linear strain formulations. The linear strain formulation gives acceptable results when Ω is smaller than 0.28.

Accuracy of One-Mode Approximation

Up to this point we have assumed that the one-mode approximation can well represent the essence of responses u and v. While this is usually the case from previous experience, it is desirable to check the accuracy of this assumption. For more accurate approximation we can assume multiple-mode expansion as

$$u(x,t)=\sum_{n=1}^{N} f_n(t)\sin\frac{(2n-1)\pi x}{2} \tag{20}$$

$$v(x,t)=\sum_{n=1}^{N} g_n(t)\sin n\pi x \tag{21}$$

where N is the number of modes used in the expansion. After substituting Eqs. (20) and (21) into Eqs. (11) and (12), multiplying Eqs. (11) and (12) by $\sin[(2n-1)\pi x/2]$ and $\sin n\pi x$, respectively, and integrating by parts from $x=0$ to 1 we obtain $2N$ equations for f_n and g_n. The Runge-Kutta method can then be used to calculate the transient response. For a two-mode approximation $N=2$, lines (2) and (3) in Fig. 11 represent g_1 and g_2, respectively when $\varepsilon=0.05$, $\mu=0$, $m_s=0.1$, $a=0.1$, and $\Omega=1$. All initial conditions are assumed to be zero. From the observation that g_2 is much smaller than g_1 in magnitude, we confirm that the first mode is much more important than the second one in approximating the solution v. The solution g from the one-mode approximation by solving Eqs. (16) and (17) is also plotted in Fig. 11 as line (1) for comparison.

Line (1) may also be compared to the result from an independent finite element calculation. Line (4) in Fig. 11 is the result obtained by a finite element method [17] retaining all high order terms in the strain energy function. From these comparisons we may conclude that the one-mode approximation can indeed retain the essence of the solutions u and v, even in the speed range of the first transverse resonance.

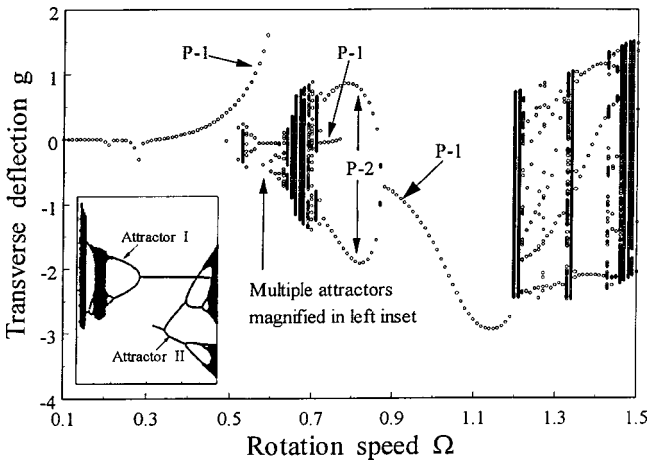

Fig. 9 Bifurcation diagram for crank length $a=0.6$. The left inset is the magnification of speed range $0.51<\Omega<0.64$.

Conclusions

We examine the steady state vibrations of a damped flexible connecting rod. Lagrangian strain formulation considering both the axial and transverse vibrations are performed to derive the

Table 1 Bifurcation speeds for attractors I and II

	Ω_{2-4}	Ω_{4-8}	Ω_{8-16}	Ω_{16-32}
Attractor I	0.54410	0.53989	0.53896	0.53874
Attractor II	0.61136	0.62661	0.63096	0.63191

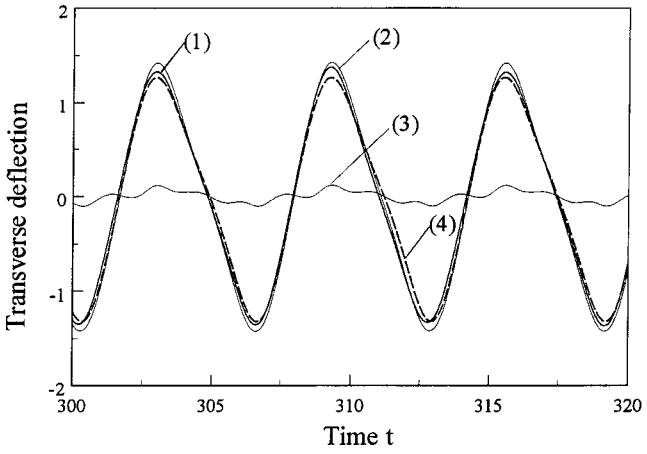

Fig. 11 Comparison of results from various calculations. Line (1): g from one-mode approximation. Lines (2) and (3): g_1 and g_2 from two-mode approximation. Line (4): g from finite element calculation. The parameters used in the calculation are $a=0.1$, $m_s=0.1$, $\varepsilon=0.05$, $\mu=0$, and $\Omega=1$.

coupled nonlinear equations of motion. The results from linear strain formulation are also presented for comparison. Several conclusions can be summarized in the following.

(1) When the crank length is small compared to the connecting rod ($a=0.1$), only periodic solutions exist in the speed range up to $\Omega=1.5$. The periodic solutions can be P-1 or P-2. Linear strain formulation gives satisfactory results when $\Omega<0.6$.

(2) For a moderate crank length ($a=0.4$), there exist multiple steady state solutions. Moreover, the response can become chaotic when $\Omega>0.86$. Linear strain formulation gives satisfactory results when $\Omega<0.3$.

(3) For a long rigid crank ($a=0.6$), chaotic response can occur as early as $\Omega=0.53$.

Acknowledgments

The results presented here were obtained in the course of research supported by a grant from the National Science Council of the Republic of China. We thank Professor T. Y. Wu of National Taiwan University for his insightful discussion on the properties of chaos.

References

[1] Neubauer, A. H., Cohen, R., and Hall, A. S., 1966, ''An Analytical Study of the Dynamics of an Elastic Linkage,'' ASME J. Eng. Ind., **88**, pp. 311–317.
[2] Badlani, M., and Kleninhenz, W., 1979, ''Dynamic Stability of Elastic Mechanism,'' ASME J. Mech. Des., **101**, pp. 149–153.
[3] Badlani, M., and Midha, A., 1982, ''Member Initial Curvature Effects on the Elastic Slider-Crank Mechanism Response,'' ASME J. Mech. Des., **104**, pp. 159–167.
[4] Badlani, M., and Midha, A., 1983, ''Effect of Internal Material Damping on the Dynamics of a Slider-Crank Mechanism,'' ASME J. Mech. Des., **105**, pp. 452–459.
[5] Tadjbakhsh, I. G., 1982, ''Stability of Motion of Elastic Planar Linkages With Application to Slider Crank Mechanism,'' ASME J. Mech. Des., **104**, pp. 698–703.
[6] Zhu, Z. G., and Chen, Y., 1983, ''The Stability of the Motion of a Connecting Rod,'' ASME J. Mech. Des., **105**, pp. 637–640.
[7] Tadjbakhsh, I. G., and Younis, C. J., 1986, ''Dynamic Stability of the Flexible Connecting Rod of a Slider Crank Mechanism,'' ASME J. Mech. Des., **108**, pp. 487–496.
[8] Viscomi, B. V., and Ayre, R. S., 1971, ''Nonlinear Dynamic Response of Elastic Slider-Crank Mechanism,'' ASME J. Eng. Ind., **93**, pp. 251–262.
[9] Hsieh, S. R., and Shaw, S. W., 1994, ''The Dynamic Stability and Nonlinear Resonance of a Flexible Connecting Rod: Single Mode Model,'' J. Sound Vib., **170**, pp. 25–49.
[10] Thompson, B. S., and Sung, C. K., 1984, ''A Variational Formulation for the Nonlinear Finite Element Analysis of Flexible Linkages: Theory, Implementation, and Experimental Results,'' ASME J. Mech. Des., **106**, pp. 482–488.
[11] Jasinski, P. W., Lee, H. C., and Sandor, G. N., 1971, ''Vibrations of Elastic Connecting Rod of a High Speed Slider-Crank Mechanism,'' ASME J. Eng. Ind., **93**, pp. 636–644.
[12] Chu, S. C., and Pan, K. C., 1975, ''Dynamic Response of a High Speed Slider-Crank Mechanism With an Elastic Connecting Rod,'' ASME J. Eng. Ind., **97**, pp. 542–550.
[13] Fung, R.-F., and Chen, H.-H., 1997, ''Steady-State Response of the Flexible Connecting Rod of a Slider-Crank Mechanism With Time-Dependent Boundary Condition,'' J. Sound Vib., **199**, pp. 237–251.
[14] Chen, J.-S., and Chen, K.-L., ''The Role of Lagrangian Strain in the Dynamic Response of a Flexible Connecting Rod,'' submitted to ASME J. Mech. Des.
[15] Hsu, C. S., 1987, *Cell-to-Cell Mapping*, Springer-Verlag, London.
[16] Moon, F. C., 1987, *Chaotic Vibrations, An Introduction for Applied Scientists and Engineers*, John Wiley and Science, New York.
[17] Chen, J.-S., and Huang, C.-L., ''Dynamic Analysis of Flexible Slider-Crank Mechanisms With Nonlinear Finite Element Method,'' accepted for publication in J. Sound Vib.